Sustainable Energy, Grids and Networks 17 (2019) 100179

Contents lists available at ScienceDirect

Sustainable Energy, Grids and Networks

journal homepage: www.elsevier.com/locate/segan

Cost and emission additionality of wind energy in power systems

Rajat Kanti Samal *, M. Tripathy

Department of Electrical Engineering, Veer Surendra Sai University of Technology Burla, Odisha, 768018, India

ARTICLE INFO

Article history:
Received 10 May 2018
Received in revised form 31 October 2018
Accepted 2 December 2018
Available online 5 December 2018

Keywords:
Cost additionality
Emission additionality
Point estimate method
Optimal power flow

ABSTRACT

Wind energy is one of the fastest growing renewable energy source (RES) to achieve energy sustainability. The existing literature is unanimous in accepting that introduction of wind energy into the power system has profound impact on power system operation more so when the penetration level is higher. In spite of this, very few attempts have been made to quantify the impact of power systems on the wind farm operation especially on the benefits of wind integration generally specified in terms of additionality and contribution to sustainable development. The term additionality here pertains to both financial and emission aspects where the impact of a wind project is compared to certain baseline scenarios as in Clean Development Mechanism (CDM). The aim of the current work is to study the impact of power systems on the cost and emission additionality of the wind farms. For this purpose three different sets of thermal generators are considered in IEEE 30 bus test system and wind farms is integrated in each of the generator systems. It is shown that the location of wind farm and the existing generator characteristics have profound impact on the additionality of wind farms. The scalability of the proposed approach is demonstrated in IEEE 118 bus 54 generator system. The approach presented in this work is novel and can be extended for quantifying the impact of power systems on more sustainability indicators of wind energy.

1. Introduction

Energy sustainability constitutes a prominent part in United Nations Millennium Development Goals [1]. The purported environmental benefits of wind energy has spurred the growth of wind industry and it has resulted in a major portion of world's energy requirement being met by wind plants. This is partly due to the encouragement and funding received from policy measures such as Clean Development Mechanism (CDM) of the Kyoto Protocol [2]. The major philosophy of such financial support is the expected sustainable development contribution of wind energy projects which has become so obvious lately. For example, in CDM, the financial assistance is based on the additionality of a CDM project which signifies that cost savings and emission reduction would not have been possible without financial assistance from CDM. The inclusion of wind energy in power systems beyond a certain level requires reconfiguration of existing power systems due to inherent nature of wind energy [3] and this impact on the power systems has garnered a lot of attention. It is feared that the introduction of renewables and associated uncertainty will force a relook at the design aspects of the power system especially the congestion aspects. But power system researchers have not given much importance to the reverse aspect i.e. how far the power system affects the additionality of a wind project, which in fact, is the very basis of existence of the wind projects. Attempts have been made to understand the factors affecting the capacity value of the wind power i.e. both inherent features such as load and wind characteristics and also subjective factors such as number of wind farms and length of wind time series [4]. A widely prevalent policy measure is to encourage wind energy developers by providing feed in tariff (FIT) and an obligation for system operators to purchase a pre-defined minimum wind energy where value factor is used to determine the correlation between power system price and the profit of wind farms [5]. But the current authors could not find any literature towards quantifying the impact of power systems on wind farm's additionality.

1.1. Motivation

Although CDM is being replaced by new frameworks such as Intended Nationally Determined Contributions (INDC) [6], the financial support for RES projects is expected to be linked with two major considerations of financial and emission additionality. Financial additionality is simply an indicator that the RES project developer cannot implement the project without external funding support. Emission additionality is the additional green house gas reduction that is expected to occur because of implementation of the project. Both the above are calculated with respect to predetermined baselines. CDM has in-built methodologies for evaluation of baseline and additionality such as ACM0002 and AMS-I.D.

* Corresponding author.
E-mail address: rajatksamal82@gmail.com (R.K. Samal).

https://doi.org/10.1016/j.segan.2018.12.001
2352-4677/

for grid connected renewable energy projects [7]. The former is for projects having capacity above 25 MW and the later is for projects having capacity less than 25 MW. It can be observed from the CDM project design documents [8] that the emission additionality is calculated simply by multiplying the average emission factor with the energy capture estimates and calculation of financial additionality is based on evaluating the internal rate of return (IRR). Both the above calculations ignore the grid integration aspects which can have substantial impact on the additionality. The current work aspires to involve power system operation in the computation of additionality which is reformulated as cost additionality (CA) and emission additionality (EA) and are defined respectively as "increase or decrease in cost or emission after integration of the wind energy into power system".

1.2. Literature survey

As discussed in the previous section, even though the cost, emission and losses are power system operational parameters, the current work studies them from a new perspective of additionality of wind farms. In order to evaluate the additionality as defined in the last section, a number of established techniques need to be reused. The following literature survey delves on (i) the concept of sustainability in smart grids, (ii) modelling wind farm uncertainty, (iii) economic emission dispatch and (iv) probabilistic optimal power flow.

Sustainability, of which financial and emission additionality are an integral part is one of the major objectives of smart grid and recent research works have attempted to address this issue. The work in [9] discusses how the components of the energy triangle viz. environmental sustainability, energy security and economic competitiveness can be achieved efficiently by distributed energy storage systems such as electric vehicles. The above work formulates the day-ahead scheduling problem involving coal, gas and wind units combined with EV charging and discharging as a mixed integer linear programming problem and uses Bender's decomposition algorithm to solve the problem. A long term generation investment model reflecting the real time systems is formulated in [10] and sensitivity analysis is performed using Monte Carlo simulation (MCS) after reducing the scenarios by Bayesian emulation. In the above work, both input uncertainty concerning variability of input parameters such as wind power and structural uncertainty involving similarity of models and real systems is taken care of and it is concluded that the uncertainties result in price volatility. The work in [11] performs generation scheduling in interconnected micro-grids where a number of objectives from prices to carbon footprint are considered and compromise solution is obtained using genetic algorithm and it is concluded that presence of distributed energy resources can reduce operational cost, emissions and improve voltage profile. An online power management system (OPM) is proposed in [12] where the objective is to reduce cost and improve dynamic response of microgrid in the presence of both non-renewable and RES and it concluded that the OPM reduces both fuel cost and emission cost. However, additionality evaluation is not explicitly considered in the above mentioned works.

In order to proceed with the endeavour of assessing the impact of power systems on the additionality of wind farms, a review of representation of wind power in power systems is required. Probability distributions (PD) are popular for representing wind uncertainty and Weibull distribution is the most preferred choice [13]. A number of parameter estimation methods are available for obtaining the parameters of the Weibull distribution from historical wind speed time series data [14]. But this has not stopped wind speed being modelled by other PDs in past literature e.g. Extreme, Weibull, Gamma, Inverse Gamma, Logistics, Log-Logistics, Inverse Gaussian distributions and both one component and two component mixture distributions [15,16]. The Beta distribution is suggested to represent wind power forecast error in [17,18]. State space models which are more general form of ARMA models are used in [19]. A conditional model to predict wind speed forecast errors is provided in [20] from which wind power scenarios can be generated. As the focus of this study is not on probability distributions and scenario generation, we adopt more common Weibull distribution for modelling wind speed uncertainty.

Since the additionality is to be expressed in terms of power system operational parameters, the second important aspect is inclusion of wind power in the economic dispatch (ED) and economic emission dispatch (EED) model and ultimately in optimal power flow (OPF) which represents the operational condition under steady state. The effort to obtain improved solutions to the ED problem is still in progress, for example, the work in [21] proposes a deterministic hybrid method based on mixed-integer linear programming (MILP). One of the most popular methods to incorporate wind power in the EED model based on underestimation and overestimation cost is proposed in [22]. A gravitational acceleration enhanced particle swarm optimization (GA-PSO) method is utilized in [23] for wind inclusion in multi-objective dispatch but the authors did not highlight the fact that in certain scenarios emission is increased after wind integration. A hybrid algorithm involving differential evolution (DE), PSO and Gaussian membership function based fuzzy selection is proposed in [24] for day-ahead EED problem where aggregated cost and emission over 24 h interval is calculated but the authors have not focused on additionality. A probabilistic ED method is suggested in [25] where the solution of the ED problem provides the PD of the output of thermal generators. An EED model incorporating carbon pricing and wind power uncertainty is proposed in [26] where it is concluded that the decision maker's judgement towards incorporating wind power can be positively influenced by increasing carbon price.

Additionality calculation may not provide practical results if the network aspects are not taken into consideration. Probabilistic OPF (POPF) incorporates uncertainty in input variables and can provide abundant information for power system planning and hence for the purpose of additionality evaluation. A number of approaches such as simulation, analytical and approximate methods have been suggested to incorporate wind uncertainty [27]. Monte Carlo simulation (MCS) method based on random numbers has been the most preferred one in which a large number of samples of uncertain variables are generated and deterministic OPF is executed for each sample. But the number of OPF runs becomes very high when the uncertain variables are large and may take lots of computational time. A combination of analytical and approximate methods is utilized in [28] to perform probabilistic load flow (PLF) and the results are compared with 10000 MCS runs. In the work [29], 5000 MCS runs are used to obtain the mean and standard deviation of power system operational parameters in IEEE 30 bus systems with wind farms integrated at buses 3, 19 and 26. Voltage security aspect is considered in [30] where FACTS devices are incorporated to provide voltage support in underestimation scenario.

The approximate methods for POPF such as point estimate method (PEM) provide sufficiently accurate results with much less computation time and complexity compared to MCS and analytical methods. It is shown in [31] that two point estimate methods (2PEM) correctly estimate the distribution of load flow solutions even under high uncertainty in bus power injections and requires only 2n calculations for n uncertain parameters [32]. For implementation of PEM, it is required to find the first four moments of the input PDFs which are mean, variance, skewness and kurtosis. The accuracy can be increased by increasing the number of estimate points and by transforming the variables to standard normal space by Rosenblatt transformation [33]. Four different PEMs are compared in unbalanced distribution system with correlated wind

and solar resources in [34] and it is concluded that accuracy does not improve significantly in higher order PEMs and 2m+1 PEM (TPEM) is the most suitable. The work in [35] uses 2m and 2m+1 PEM to model load correlation in wind integrated power systems where normal distribution is used for nodal injections and Weibull distribution for wind speed. PEM, Quasi Monte Carlo Simulation (QMCS) and latin hypercube sampling (LHS) methods of solving POPF are compared in [36]. The work in [37] uses 2m+1 PEM to perform multi-objective reactive dispatch problem where voltage deviation and losses are the conflicting objectives and conclude that the results obtained from few estimate points for PEM are comparable to those by MCS method. The author in [38] has performed the OPF for a wind-thermal-solar system connected with storage devices by incorporating wind uncertainty using 2PEM. Correlation in PEM based POPF is addressed in [39–41]. Since additionality evaluation is mostly policy related, the accuracy of PEM is acceptable and therefore this work utilizes 2m+1 PEM.

1.3. Contributions and paper organization

In the light of above discussion, the contributions of this paper are summarized below.

1. The load and wind uncertainty are incorporated in the POPF model by PEM and their impact on the cost additionality (CA) and emission additionality (EA) is investigated. The variability of CA and EA are judged by their respective coefficient of variation (CV).
2. Three different test systems having different types of generator cost and emission characteristics are chosen and the impact of the above characteristics on CA and EA is investigated. The scalability of the approach is demonstrated in a large scale fourth test system.
3. The association between the real power losses, reactive power losses, and network constraints on the CA and EA is investigated. New concepts of Real Power Loss additionality (PLA) and Reactive Power Loss Additionality (QLA) are introduced.
4. Sensitivity analysis is done by varying the rated power (P_r) and rated speed (v_r) of the wind turbines and the impact of the same on the CA, EA, PLA and QLA are studied.

It is worthwhile to put in perspective the contributions of the current work with respect to one of the earlier works by the same authors [42]. In the above mentioned work, the cost savings and emission reduction capability of the wind energy in power systems is demonstrated in four selected test power systems. However, the above work only considers the EED problem and network aspects are not included. The current work builds upon the earlier work by including the network aspects in terms of load flow and by considering both real and reactive power losses. Another novelty in this work compared to the earlier one is using point estimate method thus making the treatment of uncertainty more comprehensive. Further, whereas the earlier work includes only wind variability the current work adds load uncertainty.

2. Background

As the current study involves PEM based POPF where load and wind uncertainty are modelled by their respective PDs, a background of the above techniques are provided in this section.

2.1. Modelling uncertain variables

In the analysis of wind integrated power systems, the most important uncertain variables are load and wind power temporal variations. The load variation is generally modelled as normal distribution which basically models active power demand (P_D) and then reactive power demand (Q_D) is obtained based on a fixed power factor [40]. Based on the literature review detailed in Section 1.2, the current work uses Normal and Weibull PDs to model load and wind uncertainty respectively. The probability density function (PDF) and cumulative distribution function (CDF) of the normal distribution are provided in (1) and (2) respectively where μ and σ are the mean and standard deviation respectively. The skewness (γ_1) and kurtosis (γ_2) of normal distribution are 0 and 3 respectively.

$$f(P_d) = \frac{1}{\sigma\sqrt{2\pi}} exp\left[-\frac{(P_d-\mu)^2}{2\sigma^2}\right] \tag{1}$$

$$F(P_d) = \int_0^{P_d} \frac{1}{\sigma\sqrt{2\pi}} exp\left[-\frac{(P_d-\mu)^2}{2\sigma^2}\right] dp \tag{2}$$

The PDF and CDF of Weibull distribution are provided in (3) and (4) respectively where $f(v)$ and $F(v)$ are respectively PDF and CDF of Weibull distribution, v is the wind speed, k is the shape parameter describing the shape/width/peak of the distribution and c is the scale parameter more important in energy calculations. The mean, standard deviation, skewness and kurtosis for Weibull distribution are provided in (5a) to (5d).

$$f(v) = k\frac{v^{k-1}}{c^k} \exp\left(-\left(\frac{v}{c}\right)^k\right) \tag{3}$$

$$F(v) = \exp\left(-\left(\frac{v}{c}\right)^k\right) \tag{4}$$

$$\mu = c.\Gamma(1+1/k) \tag{5a}$$

$$\sigma = c.\left[\Gamma(1+2/k) - \Gamma^2(1+1/k)\right]^{1/2} \tag{5b}$$

$$\gamma_1 = \frac{\Gamma(1+3/k)c^3 - 3\mu\sigma^2 - \mu^3}{\sigma^3} \tag{5c}$$

$$\gamma_2 = \frac{c^4\Gamma\left(1+\frac{4}{k}\right) - 4\gamma_1\sigma^3\mu - 6\mu^2\sigma^2 - \mu^4}{\sigma^4} \tag{5d}$$

Although past literature have dwelt upon using pre-defined PDs for modelling temporal variations in load and wind speed, nevertheless, this assumptions have certain implications. For example, concerns may arise regarding the effect on the additionality due to variation in PD parameters or rather selecting an altogether new PD. However, the current authors are of the opinion that additionality evaluation generally concerns the policy level and assumption of widely used PDs to model the uncertainty can be a genuine starting point. However, based on the preference of the decision makers another PD may be chosen. In such a case, the procedure followed in the current work is still applicable as only the characteristics of the PD will change. As far as variation of the parameters are concerned, additionality evaluation is generally done for an wind farm in a selected location which has more or less similar PD parameters over the years. For a new wind farm in a different location, there may be changes in parameters of the PD thus affecting the additionality, which, however, is expected as the location has changed. A sensitivity analysis to the variation in k and c in wind-integrated ED can be found in [22].

2.2. Turbine performance index

The measured wind speed is generally at lower heights of meteorological towers and hence must be extrapolated using techniques provided in [43] to the wind turbine hub height. From these

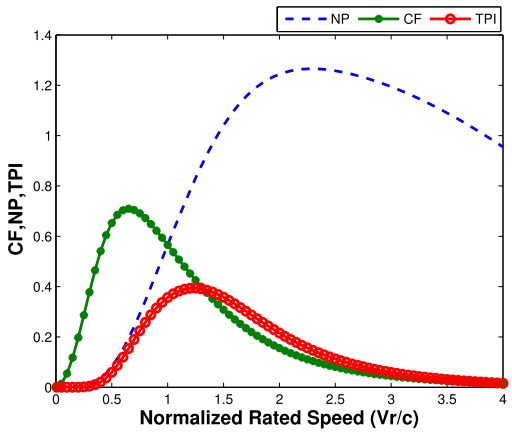

Fig. 1. Normalized power, capacity factor and TPI curves for $k = 2.2$.

wind speed values, the power output of a wind turbine can be conveniently obtained from the wind turbine power curve (WTPC) provided by the manufacturers. A number of mathematical models of wind turbine power curves are provided in [44]. The present study uses a linear power curve model provided in (6).

$$P_0 = \begin{cases} 0, & \text{for } v < v_c \\ P_r \dfrac{v - v_c}{v_r - v_c}, & \text{for } v_c < v < v_r \\ P_r, & \text{for } v_r < v < v_f \\ 0, & \text{for } v > v_f \end{cases} \tag{6}$$

where P_0 is the power output, P_r is the rated power of the wind turbine, v_r is the rated speed, v_c and v_f are cut-in speed and furling speed respectively. Since P_r is available only at v_r, choosing a turbine having higher v_r for a region with low wind regime will result in the wind turbine being operated at a fraction of P_r (normalized power (NP)) most of the time. On the contrary, choosing a lower v_r will results in loss of energy at higher speeds resulting in lower capacity factor (CF). A compromise between NP and CF can be represented by means of a turbine performance index (TPI) described in [45]. A unique TPI curve is obtained for a specific value of k as shown in Fig. 1. It can be observed from the above figure that change in v_r changes the TPI and hence energy capture which may affect the additionality.

2.3. Optimal power flow

The aim of the OPF problem is to obtain a power flow solution which optimally satisfies the stated objectives subject to all the system constraints. The objectives of OPF can be various operational aspects of the power system. The solution types significant for additionality evaluation are minimum fuel cost (MC), minimum emission (ME) and multi-objective (MO) cost and emission minimization. The OPF problem may be stated as described in Eq. (7).

$$\begin{aligned} &\textit{Minimize} \quad [F(P_i), E(P_i)] \\ &\textit{Subject to} \\ &g(P_i) = 0 \\ &h(P_i) \le 0 \end{aligned} \tag{7}$$

where

$$F = \sum_{i=1}^{N} a_i + b_i P_i + c_i P_i^2 + |d_i sin\left(P_i^{min} - P_i\right)^2| \tag{8}$$

$$E = \sum_{i=1}^{N} \alpha_i + \beta_i P_i + \gamma_i P_i^2 + \eta_i exp\left(\delta_i P_i\right) \tag{9}$$

$$\sum_{i=1}^{N} P_i = P_D + P_L \tag{10}$$

$$P_i^{min} \le P_i \le P_i^{max} \tag{11}$$

$$S_l \le S_l^{max} \tag{12}$$

$$((V_i)^2)^{min} \le (e_i^2 + f_i^2) \le ((V_i)^2)^{max} \tag{13}$$

where F is the fuel cost of generation in ($/h); E is the emission in (ton/h or lb/h); N is the number of thermal generators; for an ith generator P_i is the real power output; a_i, b_i, c_i, d_i and e_i are the coefficients of the fuel cost characteristics; α_i, β_i, γ_i, η_i and δ_i are the coefficients of emission characteristics. $g(P_i)$ and $h(P_i)$ are the system equality and inequality constraints respectively. Similarly, P_D and P_L respectively represent the total electric power demand and total real power loss in the transmission lines. S_l is the total power transfer through the lth line and V_i is the bus voltage of the ith system bus.

The variation in wind power injection is uncertain and can be included in the dispatch model by using the underestimation and overestimation cost models presented in [22] and reproduced in (14).

Minimize

$$\sum_{i=1}^{N} C_i\left(P_i\right) + \sum_{i=1}^{M} C_{w_i}\left(w_i\right) + \sum_{i=1}^{M} C_{pwi}\left(W_{i,av} - w_i\right) + \sum_{i=1}^{M} C_{rwi}\left(w_i - W_{i,av}\right) \tag{14}$$

Subject to

$$\begin{aligned} &P_i^{min} \le P_i \le P_i^{max} \\ &0 \le w_i \le w_{r,i} \\ &\sum_{i=1}^{N} P_i + \sum_{i=1}^{N} w_i = P_D + P_L \end{aligned} \tag{15}$$

In the above equations,

N is the number of thermal generators,

M is the number of wind powered generators,

w_i and $W_{i,av}$ respectively are the scheduled and available values of real power from the ith wind generator

$w_{r,i}$ rated wind power from the ith wind powered generator.

C_i is the cost function of the ith conventional generator

C_{w_i} is the cost function of the ith wind generator

C_{pwi} and C_{rwi} respectively are the penalty cost function for not using all the available wind power and reserve cost function associated with overestimation of wind power, both for the ith wind powered generator. The direct cost is assumed to be a linear function of generated wind power as given in Eq. (16).

$$C_{w_i} = g_i \times w_i \tag{16}$$

where g_i is the direct cost coefficient ($/MWh) of the wind generator. As the penalty and reserve cost functions penalize wind deviations, these can be represented as shown in (17) and (18) respectively.

$$C_{pwi}(w) = c_p|W_{i,av} - w_i| = c_p \int_{w_i}^{W_{i,rated}} (w - w_i) f_W(w) dw \tag{17}$$

$$C_{rwi}(w) = c_r|w_i - W_{i,av}| = c_r \int_{w_i}^{W_{i,rated}} (w_i - w) f_W(w) dw \tag{18}$$

where f_W denotes the PDF of wind power, c_p is the penalty cost coefficient, c_r is the reserve cost coefficient, $W_{i,rated}$ is the rated power of the ith wind generator.

2.4. Point estimate method

As compared to simulation method, the PEM obtains selected estimate points of the uncertain variables and their weights. These estimate points are then utilized for performing deterministic OPF. Finally the results are combined by using the weights of estimate points to obtain PDF of the output variables. A summary of the number of points and their weights can be obtained from [39]. As discussed in Section 1.2, 2m+1 PEM is found to provide most satisfactory results and is adopted for this work. A brief overview of 2m+1 PEM is provided below [40].

In 2m+1 PEM, each random variable (RV) is represented by three locations determined by (19).

$$y_{ik} = \mu_i + \zeta_{i,k}\sigma_i \tag{19}$$

where i = 1,2,…,m is the number of uncertain input variables, k = 1,2,3 is the number of estimate points, μ and σ are the mean and standard deviation of the PDF of the marginal distribution of the uncertain variable. $\zeta_{i,k}$ is used to obtain the location of kth estimate point of the ith uncertain variable and is obtained by (20).

$$\zeta_{ik} = \frac{\gamma_{1,i}}{2} + (-1)^{3-k}\sqrt{\gamma_{2,i} - \frac{3}{4}\gamma_{1,i}^2} \tag{20}$$

where k = 1,2 and $\zeta_{i,3} = 0$ which represents the mean value, $\gamma_{1,i}$ and $\gamma_{2,i}$ are respectively skewness and kurtosis of the respective marginal distributions of the uncertain variables. Weights for each of the estimate points are given by (21a) and (21b).

$$w_{i,k} = \frac{(-1)^{3-k}}{\zeta_{i,k}(\zeta_{i,1} - \zeta_{i,2})}\ (k = 1, 2) \tag{21a}$$

$$w_{i,3} = \frac{1}{m} - \frac{1}{\gamma_{2,i} - \gamma_{1,i}^2} \tag{21b}$$

Once the concentration points are found 2m+1 vectors of input variables are obtained as in (22a) for k = 1,2,…,m and (22b) for k = 2m + 1 which the all mean input vector.

$$Y_j(i,k) = [\mu_1, \mu_2, \mu_3, \ldots, \mu_{i-1}, y_{i,k}, \mu_{i+1}, \ldots, \mu_m] \tag{22a}$$

$$Y_{2m+1} = [\mu_1, \mu_2, \ldots \mu_m] \tag{22b}$$

The 2m+1 vectors of input RVs are used to solve 2m+1 deterministic OPF and the solution vector Z obtained for each such OPF is combined using the estimate point weights by using (23a) to (23c) for obtaining the PDFs of output variables.

$$\mu_n = \sum_{i=1}^{m}\sum_{k=1}^{3} w_{i,k}(Z_n(i,k)) \tag{23a}$$

$$E\left[Z_n(i,k)^2\right] = \sum_{i=1}^{m}\sum_{k=1}^{3} w_{i,k}(Z_n(i,k)^2) \tag{23b}$$

$$\sigma_n = \sqrt{E\left[Z_n(i,k)^2\right] - E\left[Z_n^2\right]} \tag{23c}$$

where n is the number of output variables and μ_n and σ_n are the mean and standard deviation of the nth output variable.

3. Problem formulation

The exact problem setup to obtain additionality is to evaluate the terms defined in (24a) to (24d) for the selected test systems. The terms are described below. A pictorial representation of the problem in provided in Fig. 2.

1. *Cost Additionality (CA)*: it is defined as the difference between the costs before (C_{bw}) and after (C_{aw}) wind integration as a percentage of cost before wind integration (24a).

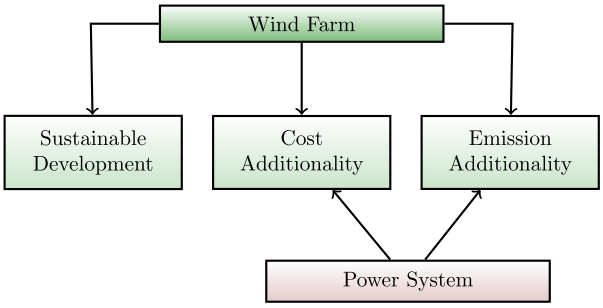

Fig. 2. Pictorial representation of the problem.

2. *Emission Additionality (EA)*: it is defined as the difference between emission before (E_{bw}) and after (E_{aw}) wind integration as a percentage of emission before wind integration (24b).
3. *P Loss Additionality (PLA)*: it is defined as the difference between real power loss before ($P_{L,bw}$) and after ($P_{L,aw}$) wind integration as a percentage of P_L before wind integration (24c).
4. *Q Loss Additionality (QLA)*: it is defined as the difference between reactive power loss before ($Q_{L,bw}$) and after ($Q_{L,aw}$) wind integration as a percentage of Q_L before wind integration (24d).

$$\text{CA} = \frac{C_{bw} - C_{aw}}{C_{bw}} \text{ x } 100 \tag{24a}$$

$$\text{EA} = \frac{E_{bw} - E_{aw}}{E_{bw}} \text{ x } 100 \tag{24b}$$

$$\text{PLA} = \frac{P_{L,bw} - P_{L,aw}}{P_{L,bw}} \text{ x } 100 \tag{24c}$$

$$\text{QLA} = \frac{Q_{L,bw} - Q_{L,aw}}{Q_{L,bw}} \text{ x } 100 \tag{24d}$$

In addition, to appreciate the variations in additionality due to input uncertainty, the coefficient of variation (CV) of cost (CCV), emission (ECV), P_L (PLCV) and Q_L (QLCV) are also evaluated using (25).

$$CV = \frac{\mu}{\sigma} \tag{25}$$

where CV is the coefficient of variation, μ and σ are mean and standard deviation of the selected variable.

4. Solution methodology

The solution steps are described below. The same is shown pictorially in Fig. 3.

1. For each of the test systems, the MC, ME and MO solutions are obtained without incorporating wind power. These solutions constitute the base case to which the corresponding wind integrated results are to be compared.
2. The estimate points for load and wind variations are obtained from Normal and Weibull distributions using (19) and (20). The corresponding weights of the estimate points are obtained by using (21a) and (21b).
3. Input vectors for each of load variation, wind variation and their combination are obtained using (22a) and (22b) and deterministic OPF is solved for each of the input vectors.
4. The results obtained from deterministic OPFs are combined using (23a) to (23c) to obtain the mean and CV of the cost, emission, P_{loss} and Q_{loss}.

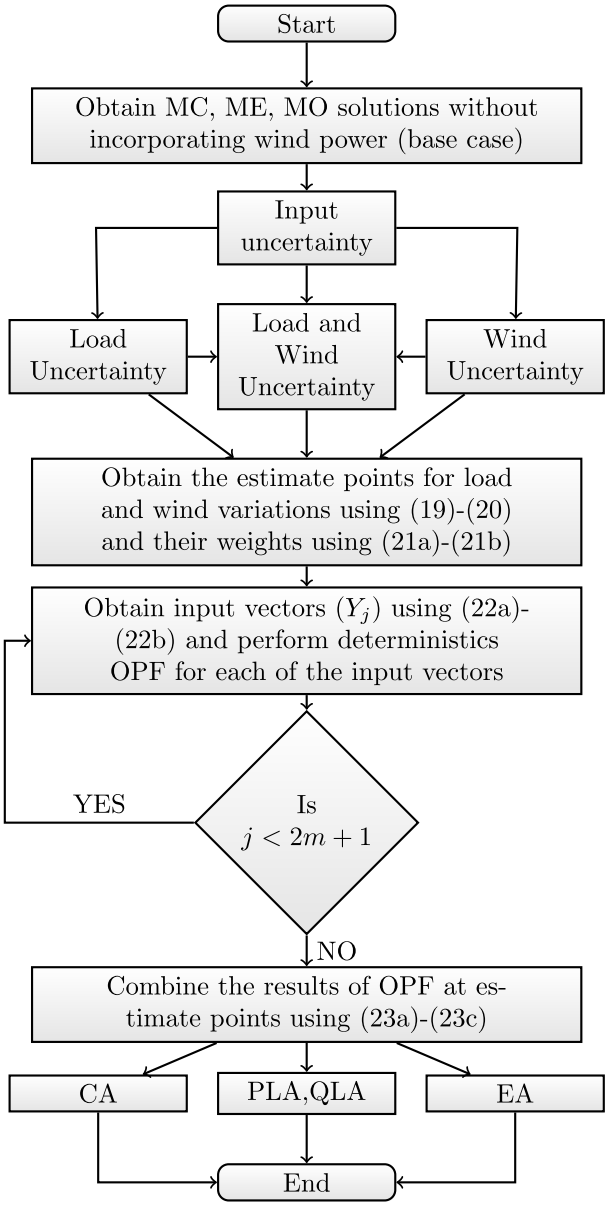

Fig. 3. Solution methodology.

5. The additionality terms defined in (24a) to (24d) are evaluated by comparing the results after wind integration with that before wind integration. The coefficient of variation of the results are obtained using (25).

Since the focus of this work is not on optimization, the `fmincon` function of MATLAB Optimization Toolbox is used to obtain the MC and ME solutions and the `gamultiobj` function of MATLAB Global Optimization Toolbox is used to obtain the MO solution. For MO solution of the large scale test system `fgoalattain` is utilized to reduce the computation time. Matpower 5.1 [46] is used to perform the load flow. It is worthwhile to mention here the rationale behind not trying to reach the global optimum. The authors believe that this is not required as the core of the work lies in comparing results with and without wind integration. However, concern may arise in reader's mind about the difference in quality of solutions with the state-of-the-art and those with the selected methodologies. We agree that since the MC, ME, MO solutions are compared across different scenarios, the quality of the solution nevertheless matters. To alleviate such concerns, the readers may refer [42] for a comparison of the results of the state-of-the-art and those obtained using MATLAB functions where it is demonstrated that both are comparable and have no difference from a practical perspective.

Table 1
Description of the scenarios.

Scenario	Section	Wind	Load
1	5.1	No wind	Deterministic
2	5.2	No wind	Stochastic
3	5.3	Stochastic	Deterministic
4	5.4	Different P_r	Deterministic
5	5.5	Different v_r	Deterministic
6	5.6	Stochastic	Stochastic

Table 2
Generation Schedule (MW) for Scenario 1 (No Wind).

Test system	Solution type	P_{g1}	P_{g2}	P_{g3}	P_{g4}	P_{g5}	P_{g6}
TS-1	MC	11.34	30.27	53.32	102.22	53.32	36.33
	ME	40.96	46.29	54.34	38.92	54.34	51.45
	MO	34.07	44.64	50.06	64.36	54.16	39.05
TS-2	MC	192.48	48.45	19.57	11.74	10.00	12.00
	ME	113.87	46.85	34.70	30.57	29.99	32.83
	MO	142.34	52.83	30.69	21.95	17.69	25.09
TS-3	MC	41.08	47.44	35.02	35.01	35.01	94.28
	ME	51.96	44.92	45.44	52.37	41.43	50.62
	MO	49.09	44.23	37.46	78.49	35.48	42.35

5. Results and discussion

The details of the cost and emission characteristics of the generators for TS-1 to TS-3 are provided in Tables A.1 to A.3 in the Appendix. The generators of the test system 1 (TS-1) [23] have quadratic cost characteristics and the emission characteristics have non-linear terms. The generators of the test system 2 (TS-2) [40] have quadratic characteristics for both cost and emission. The generators of the test system 3 (TS-3) [24] have valve point loading effect in the cost characteristics and non-linearities in the emission characteristics. A large scale fourth test system (TS-4), which is IEEE 118 bus 54 generator system, is also included to demonstrate the scalability of the proposed approach. The generator data of TS-4 are obtained from [47] and the load and network details are obtained from [46]. The nominal load for the first three test systems are 283.4 MW and that of TS-4 is 4242 MW. For scenarios concerning load variations, the active load at the buses are assumed to have a variance of 10% of the mean. The mean P_d values are provided in Tables B.1 and B.2 in Appendix. The power factor is assumed to be 0.85 and reactive power demands (Q_d) are obtained accordingly. For ready reference of the readers, a summary of the various scenarios considered are provided in Table 1. For TS-4, only the first three scenarios are considered since this suffices to demonstrate the scalability.

5.1. Scenario 1: Base scenario (No wind)

Initially the OPF is performed without wind integration for all the test systems. Although the results are available in the existing literature, the same is obtained using the tools selected for the current work so that additionality can be properly calculated. The generation schedule for TS-1 to TS-3 without wind integration are provided in Table 2. The cost and emission for TS-1 to TS-4 are provided in Table 3. As the load is same for the first three test systems, the generation schedule, cost, emission, P_{loss} and Q_{loss} for different sets of generator characteristics can be easily compared and the differences can be appreciated.

Table 3
Cost and emission for Scenario 1 (No Wind).

Test system	Solution type	Cost ($/h)	Emission (ton/h)	P_{loss} (MW)	Q_{loss} (MVAR)
TS-1	MC	607.67	0.2222	3.41	20.83
	ME	644.85	0.1942	2.89	20.50
	MO	623.09	0.1983	2.94	19.68
TS-2	MC	805.70	0.4627	10.84	42.64
	ME	852.27	0.3333	5.42	23.76
	MO	819.51	0.3571	7.19	29.23
TS-3	MC	3096.26	3.6846	4.43	29.31
	ME	3441.86	2.2767	3.34	19.14
	MO	3121.88	2.8683	3.68	18.83
TS-4	MC	54 821	1 865 360	152.24	754.30
	ME	56 831	1 171 960	90.18	437.70
	MO	55 463	1 177 735	137.60	673.59

Table 4
Mean of cost, emission and losses for Scenario 2.

Test system	Solution type	Cost ($/h)	Emission (ton/h)	P_{loss} (MW)	Q_{loss} (MVAR)
TS-1	MC	608.42	0.2222	3.74	22.22
	ME	645.59	0.1942	3.22	21.90
	MO	616.20	0.2018	3.20	21.22
TS-2	MC	806.99	0.4636	11.20	44.16
	ME	853.58	0.3340	5.75	25.14
	MO	883.34	0.3588	5.49	24.23
TS-3	MC	2988.17	5.2421	3.31	17.96
	ME	3445.49	2.2890	3.67	20.52
	MO	3203.85	2.8578	4.22	21.23
TS-4	MC	54 841	1 867 257	153.96	761.44
	ME	56 849	1 171 965	91.48	442.95
	MO	55 169	1 638 226	151.84	747.48

Table 5
CV (%) of cost, emission and losses for Scenario 2.

Test system	Solution type	Cost ($/h)	Emission (ton/h)	P_{loss} (MW)	Q_{loss} (MVAR)
TS-1	MC	0.89	0.03	1.71	1.63
	ME	0.84	0.02	1.83	1.60
	MO	0.94	0.53	2.45	2.30
TS-2	MC	1.11	1.54	1.72	1.58
	ME	1.10	1.32	1.78	1.51
	MO	4.57	1.82	23.74	17.00
TS-3	MC	1.43	12.87	29.61	26.44
	ME	0.80	3.75	2.01	1.71
	MO	1.66	8.46	6.12	4.37
TS-4	MC	0.15	0.41	0.54	0.51
	ME	0.14	0.0017	0.34	0.30
	MO	0.88	18.77	2.20	2.87

5.2. Scenario 2: Load variations

In the first scenario, the load is assumed to be varied according to normal distribution with standard deviation as 10% of the mean. As seen from Table B.1, for TS-1 to TS-3, 21 out of 30 buses have non-zero load. Therefore the number of estimate points are 43. For the large scale system, 99 out of 118 buses have non-zero load resulting in 199 estimate points. Deterministic OPF is performed for the input vectors obtained from these estimate points and the mean and CV of the results are obtained as per the procedure enumerated in Section 2.4. The mean and CV of cost, emission and losses are provided in Tables 4 and 5 respectively. It can be observed that for TS-1, cost increases for both MC and ME solutions whereas cost decreases for MO solution compared to fixed load i.e. base case scenario. For TS-2, cost increase has resulted in all types of solutions. For TS-3, increase in cost occurs in ME and MO solutions whereas for MC solution there is a decrease in cost with load variation. Similar pattern can be observed for emission and losses. For the large scale test system TS-4, very small increase in cost can be observed for MC, ME solution whereas the emission increases for all types of solution the largest increase being for MO solution. Losses are increased for all types of solution for load variation in TS-4. Thus it can be concluded that the response of different test systems to load variations is quite different and the solution type viz. MC, ME or MO influences the impact of load variation on cost, emission and losses.

Table 6
Location of the wind farms (TS-1, TS-2, TS-3).

Loc#	1	2	3	4	5	6	7
Bus#	3,4	6,9	14,15	22,25	26,30	27,28	29,30

Table 7
Location of the wind farms in TS-4.

Loc#	Bus number
1	20, 21, 22, 23, 28, 29, 30, 33
2	37, 38, 39, 43, 44, 45, 47, 48
3	50, 51, 52, 53, 57, 58, 63, 64
4	71, 75, 78, 79, 81, 82, 83, 84

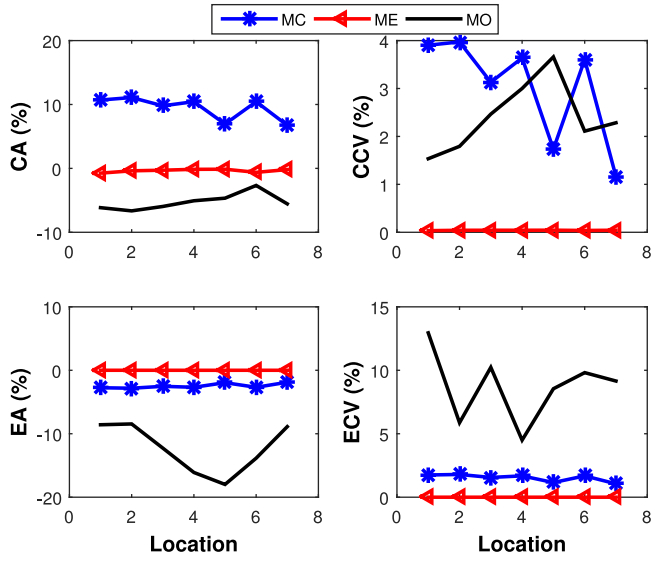

Fig. 4. Cost and emission additionality in TS-1 (Scenario 3).

5.3. Scenario 3: Wind variations

In this scenario, the load is fixed and point estimates for the wind power are obtained. Two wind farms are assumed to be integrated at two different buses of the IEEE 30 bus system. Thus the total number of estimate points for wind variation is 5. The wind speed is assumed to follow Weibull distribution with shape and scale parameters of 2.2 and 15 m/s respectively. The P_r, v_c, v_r and v_f of the wind turbines are assumed to be 1.5 MW, 3 m/s, 12 m/s and 25 m/s respectively. Each wind farm consists of 50 wind turbines and a linear power curve is assumed. Thus each wind farm has an installed capacity of 75 MW resulting in total wind IC to be 150 MW in the power system. The location of the wind farms are varied and for each location additionality and CV are obtained. The locations are provided in Table 6. For the large scale test system, eight wind farms are integrated at four different sets of locations provided in Table 7. Thus in TS-4, the total IC is 600 MW which is 14.14% of the total system load.

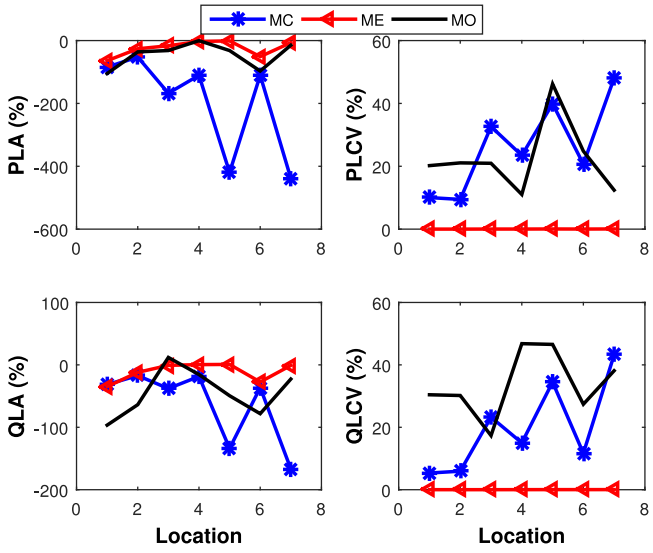

Fig. 5. Loss additionality in TS-1 (Scenario 3).

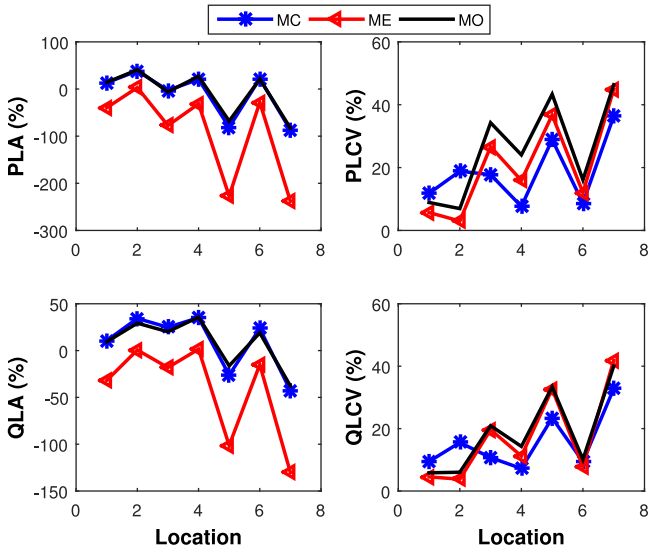

Fig. 7. Loss additionality in TS-2 (Scenario 3).

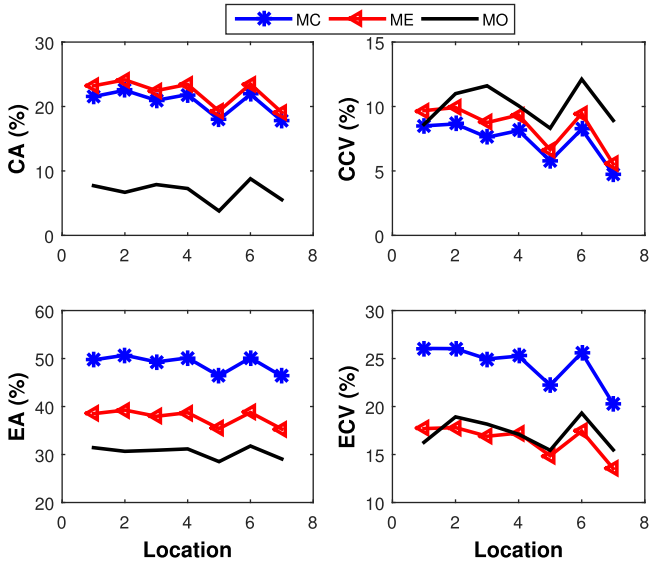

Fig. 6. Cost and emission additionality in TS-2 (Scenario 3).

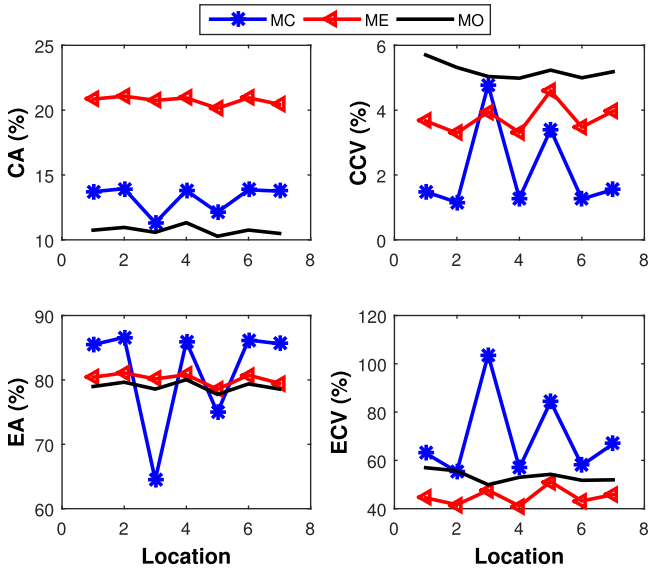

Fig. 8. Cost and emission additionality in TS-3 (Scenario 3).

5.3.1. Test system 1

It can be observed from Fig. 4 that the CA is positive only for MC solution and hence ME and MO solution have resulted in increase in fuel cost after wind integration. The CCV has a maximum value of 4% when the wind farm location is changed. It can also be observed that the EA does not vary much for MC and ME solutions, however up to 18% decrease in emission occurs with MO solution. The CA is highest at 11% when the wind farm is located at buses 6, 9 and for MC solution. The highest value of EA is nearly zero for MC and ME solutions and is almost same for all locations. The negative value of PLA and QLA in Fig. 5 shows that wind integration has resulted in more real and reactive losses for all types of solution.

5.3.2. Test system 2

The CA and EA for TS-2 after wind integration at various locations are provided in Fig. 6. Contrary to TS-1, the both the CA and EA of wind farms are very high when integrated in TS-2. The highest CA of 24.1% occurs for ME solution and the lowest CA is at 3.8% for MO solution. The EA of MC solution is the highest followed by ME and MO solutions for all locations. As observed from Fig. 7, the PLA, QLA have followed similar patterns as in TS-1.

5.3.3. Test system 3

As can be seen from Fig. 8, the CA values are the highest for ME solution followed by MC and MO solutions. The EA of wind farms when integrated with TS-3 is very high, the maximum and minimum being 86.6% for location 2 and 64% for location 3 respectively, both occurring in case of MC solution. It can be observed from Fig. 9 that the PLA is still negative though less severe as compared to previous two test systems.

5.3.4. Test system 4

The CA and EA for the TS-4 after wind integration at four different sets of buses are provided in Figs. 10 and 11 respectively. It can be observed from Fig. 10 that the CA and CCV varies across locations; location change does not seem to have any effect on EA. Change in location of wind farms has impact on ECV only for MO solution. As seen from Fig. 11, mean and coefficient of variation of losses vary widely across locations (see Figs. 13 and 15).

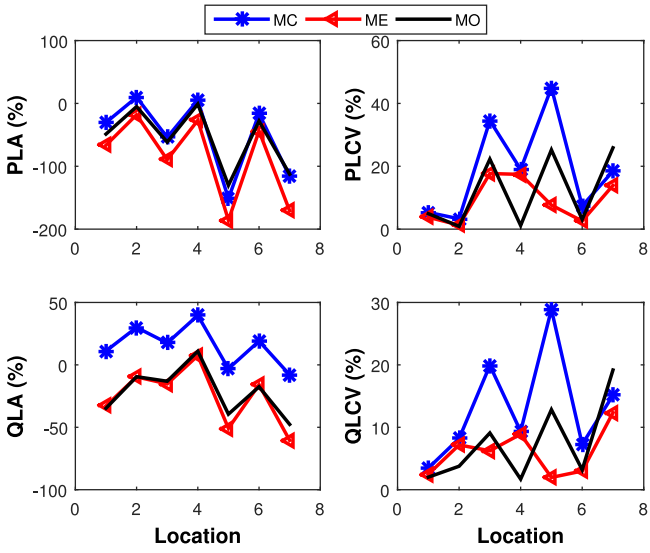

Fig. 9. Loss additionality in TS-3 (Scenario 3).

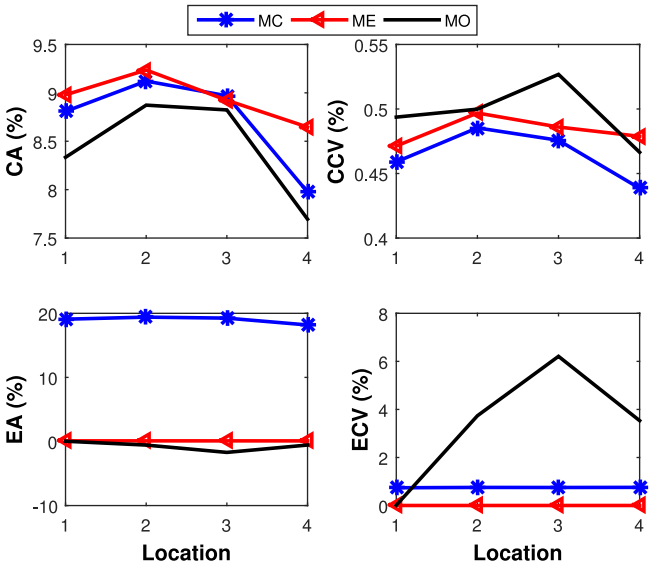

Fig. 10. Cost and emission additionality in TS-4 (Scenario 3).

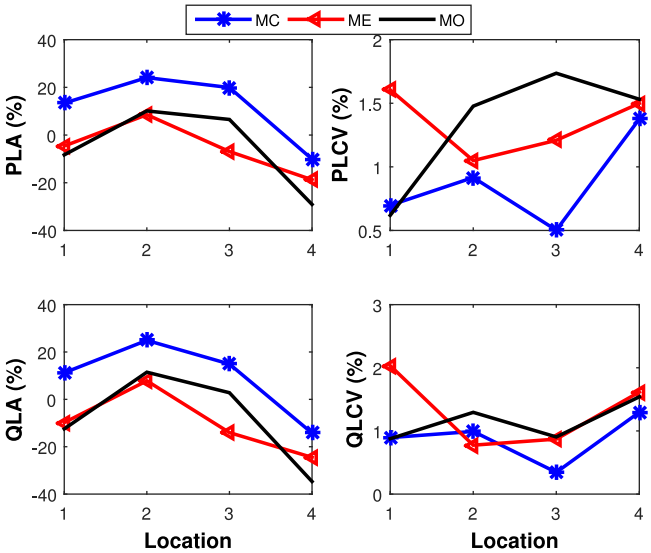

Fig. 11. Loss additionality in TS-4 (Scenario 3).

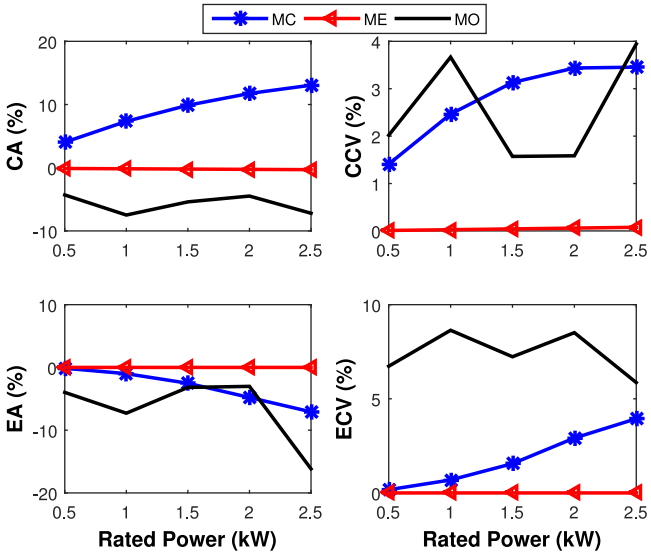

Fig. 12. Cost and emission additionality in TS-1 (Scenario-4).

5.4. Scenario-4: Sensitivity analysis to P_r

In this scenario, the location of the wind farms are fixed at buses 14, 15 and the P_r of the wind turbines is varied from 0.5 MW to 2.5 MW in steps of 500 kW. This results in capacity of each wind farm changing from 25 MW to 125 MW in steps of 25 MW. For each P_r, five estimate points are obtained and OPF is performed for each of the estimate points.

5.4.1. Test system 1

From Fig. 12, it is observed that with increase in P_r, the CA increases from 4% to 13%, decreases from −0.12% to −0.31% and decreases from −4.30% to −7.20% respectively for MC, ME and MO solution respectively. The EA decreases from −0.13% to −7.08% for MC solution, remains same at 0% for ME solution and varies from −4% to −16% for MO solutions. It is observed from Fig. 13 that the losses have increased with increase in P_r evident by the increasing negative values of PLA for increasing P_r for MC solution. However, PLA remains constant for ME and MO solutions. Similar variation is observed for QLA.

5.4.2. Test system 2

As seen from Fig. 14, The CA increases from 8.3% to 27% for MC solution, increase from 8.5% to 29.5% for ME solution and from −4.3% to 7.03% for MO solution. The EA follows similar pattern and increase from 20% to 61% for MC solution, 15% to 50% for ME solution and from 12% to 37% for MO solution. The real power losses have increased with increase in P_r as verified from the negative PLA values in Fig. 15. The reactive losses, however, tend to decrease.

5.4.3. Test system 3

The CA, EA and PLA, QLA values for TS-3 are provided in Figs. 16 and 17 respectively. In this test system the highest CA occur for ME solution which increases from 10% to 22%. The CA values for MC and MO solutions vary from 6% to 14% and 2% to 9% respectively. The EA varies between 22% and 90% for MC solution, between 42% and 87% for ME solution and between 48% and 80% for MO solution. The real power losses have increased for all types of solution resulting in increased negative values of PLA as the P_r

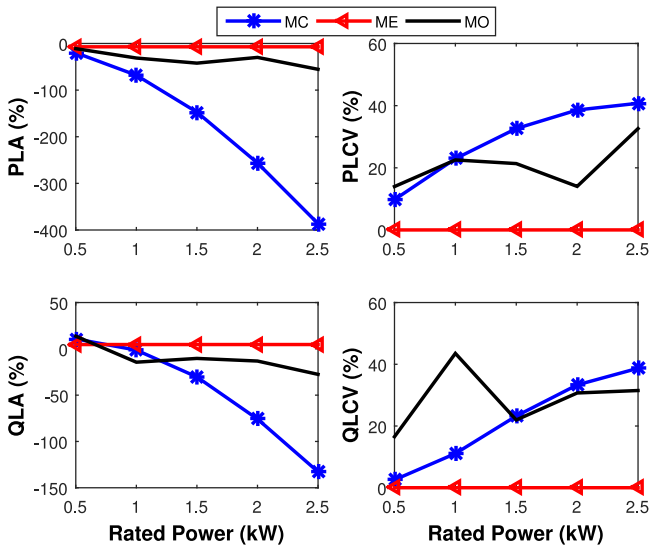

Fig. 13. Loss additionality in TS-1 (Scenario-4).

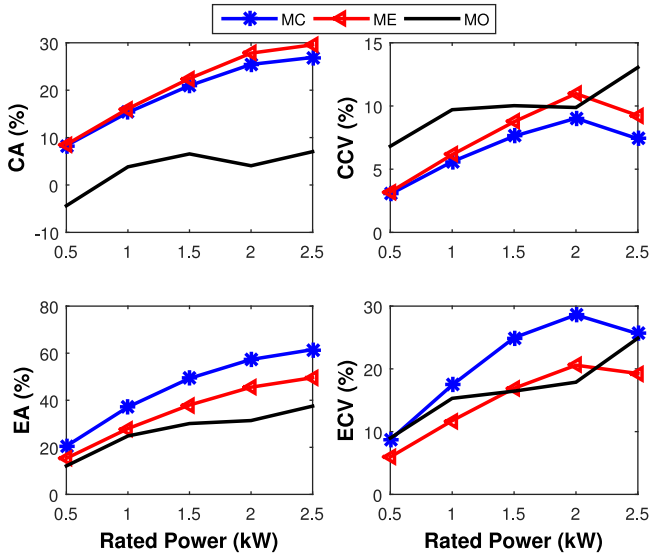

Fig. 14. Cost and emission additionality in TS-2 (Scenario-4).

increases. For TS-3, the reactive losses also tend to increase with increased P_r as interpreted from increased QLA.

5.5. Scenario-5: Sensitivity analysis to V_r

In this scenario the wind turbine ratings are fixed at $P_r = 1.5$ MW, thus making the total installed capacity of each wind farm as 75 MW. The wind farms location is fixed at bus 14, 15. The wind turbine v_r is varied from 10 m/s to 18 m/s in steps of 2 m/s thus changing the TPI as shown in Fig. 1. The CA, EA and PLA, QLA for TS-1 to TS-3 are shown in Figs. 18 to 20 respectively. It can be observed from Fig. 18 that for MC solution, CA is reduced from 11% to 7.4%, EA in increased from −3.5% to −1.2%, both real and reactive power losses have decreased even though PLA, QLA continue to be negative. The ME solution does not seem to have any impact on the additionality. For MO solution, no clear trend is visible but the additionality varies with change in v_r. As observed from Fig. 19, CA and EA have decreased whereas PLA and QLA have increased with increase in v_r. As shown in Fig. 20, the trends for TS-3 are quite similar to that in TS-2 but the variation is not linear for all types

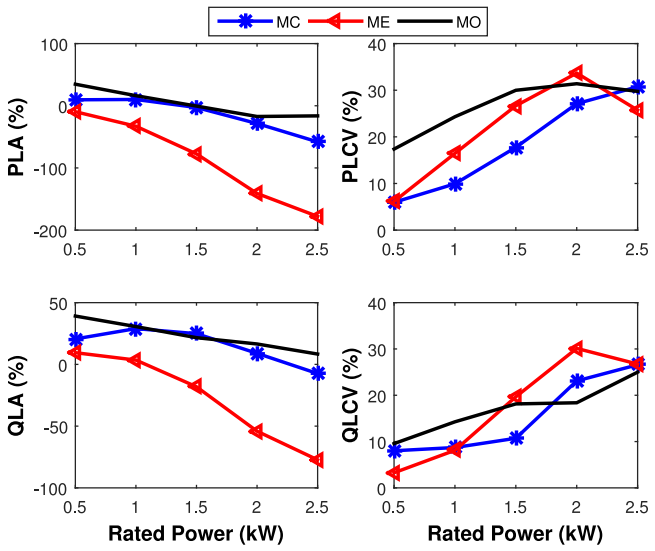

Fig. 15. Loss additionality in TS-2 (Scenario-4).

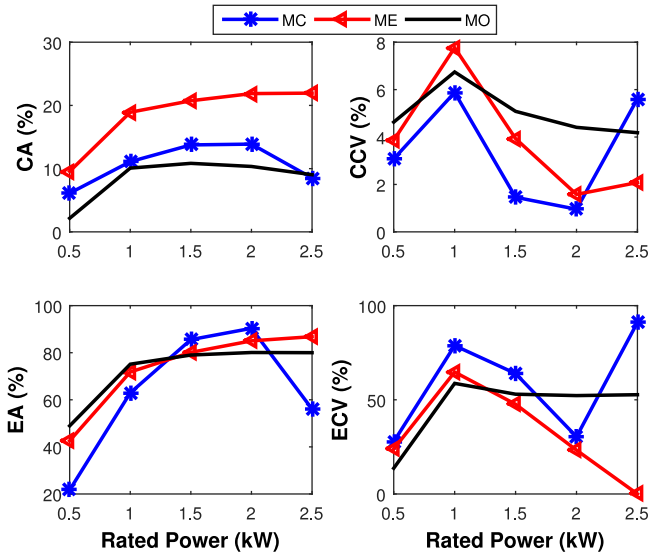

Fig. 16. Cost and emission additionality in TS-3 (Scenario-4).

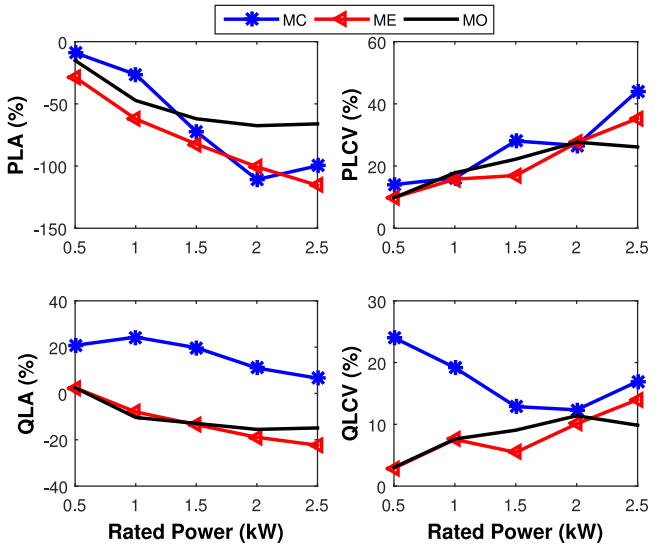

Fig. 17. Loss additionality in TS-3 (Scenario-4).

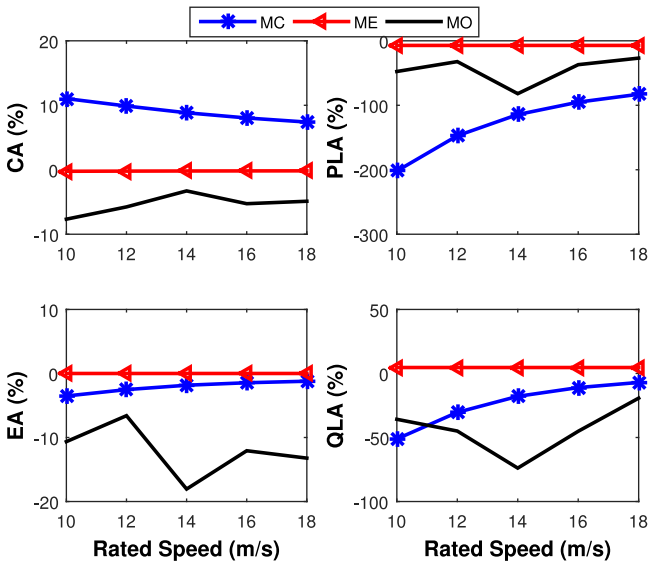

Fig. 18. Additionality in TS-1 (Scenario-5).

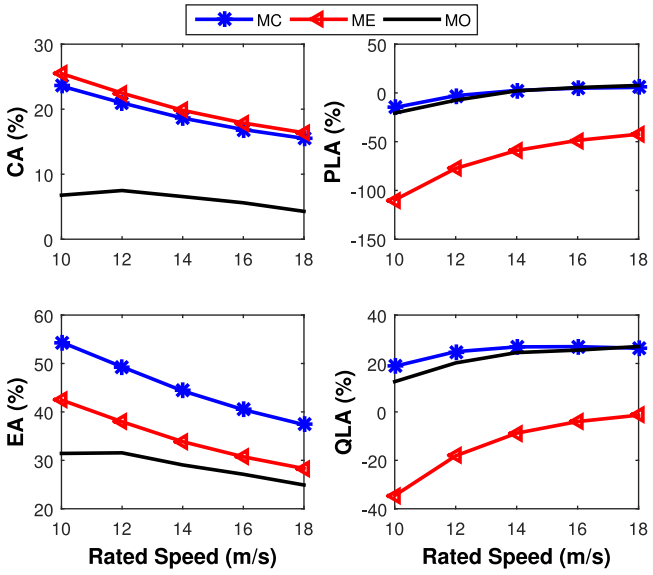

Fig. 19. Additionality in TS-2 (Scenario-5).

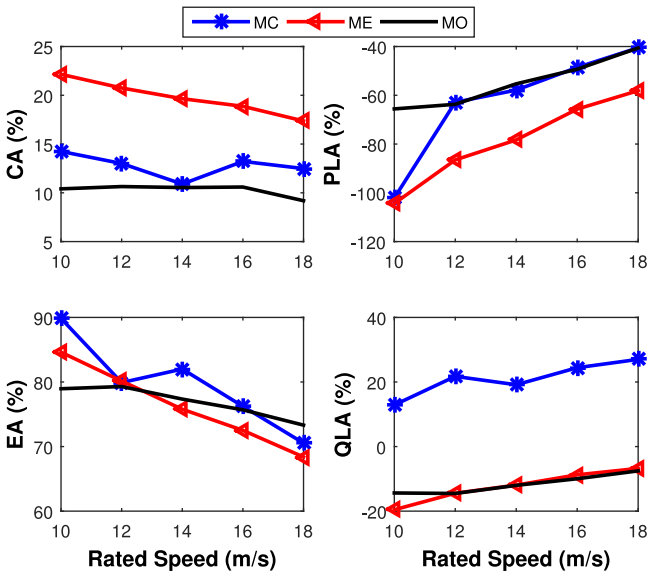

Fig. 20. Additionality in TS-3 (Scenario-5).

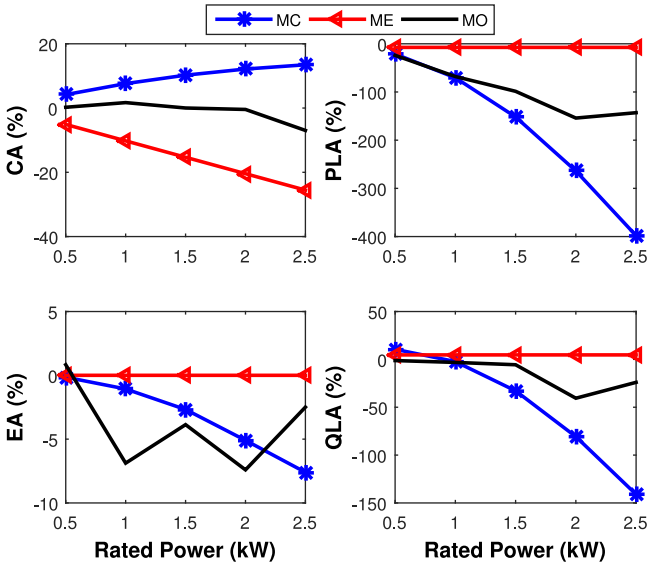

Fig. 21. Additionality in TS-1 (Scenario-6).

of solution. Also, it can be observed from above figures that the variation is additionality with change in v_r is very small compared to that due to change in P_r for all the test systems.

5.6. Scenario-6: Load and wind variations

So far, with wind integration, we have fixed the load at the buses at their mean value. In this scenario the load is varied for 21 buses as in scenario 2. In addition, two wind farms are incorporated at bus 14, 15. This increases the total number of uncertain variables to 23. Hence, according to $2m + 1$ PEM, the total number of input vectors is 47. Even though the wind variation occurs at two buses only, the weights of the scenarios are obtained by dividing the uncertainty equally between load variation and wind generation. As the readers may have some concerns regarding allotment of equal weights to load and wind uncertainty, a justification of the same is provided below. The purpose of this section is to understand the impact of both wind and load variations. As load may be available at a number of buses and wind farms only at few buses, strict distribution of uncertainty may results in load variations outweighing the wind variations. In such a case the results will be same as those which consider only load variations. Therefore, the current authors are of the opinion that sharing the uncertainty equally between wind and load variations in spite of large difference in the number of variables, is required so that the impact of concurrent load and wind variations can be investigated.

Figs. 21 to 23 respectively show the additionality for TS-1 to TS-3 respectively. It can be observed from Fig. 21 that with increase in P_r, MC solution results in increase in CA from 4.2% to 13.5%, decrease in EA from −0.2% to −7.6% and decrease in both PLA and QLA; ME solution results in decrease in CA from −5% to −25% with no change in EA, PLA and QLA; MO solution results in variation in additionality with no clearly visible trend. In TS-2, as observed from Fig. 22, all types of solution result in increase in CA, EA and decrease in PLA, QLA. As observed from Fig. 23 additionality terms in TS-3 vary similar to those for TS-2.

Table A.1
Cost and emission coefficients of the thermal generators for TS-1.

Gen#	P_i^{max} (MW)	P_i^{min} (MW)	a_i ($/h)	b_i ($/MWh)	c_i ($/(MW^{2}h))	α_i (ton/h)	β_i (ton/MWh)	γ_i (ton/MW^{2}h)	η_i (ton/h)	δ_i (1/MW)
1	50	5	10	200	100	4.091	−5.554	6.490	2.0E−4	2.857
2	60	5	10	150	120	2.543	−6.047	5.638	5.0E−4	3.333
3	100	5	20	180	40	4.258	−5.094	4.586	1.0E−6	8.0
4	120	5	10	100	60	5.326	−3.550	3.380	2.0E−3	2.0
5	100	5	20	180	40	4.258	−5.094	4.586	1.0E−6	8.0
6	60	5	10	150	100	6.131	−5.555	5.151	1.0E−5	6.667

Table A.2
Cost and emission coefficients of the thermal generators for TS-2.

Gen#	P_i^{max} (MW)	P_i^{min} (MW)	a_i ($/h)	b_i ($/MWh)	c_i ($/(MW^{2}h))	α_i (kg/h)	β_i (kg/MWh)	γ_i (kg/MW^{2}h)
1	250	50	0	2.00	0.00375	22.983	−1.1000	0.0126
2	80	20	0	1.75	0.01750	22.313	−0.1000	0.0200
3	50	15	0	1.00	0.06250	25.505	−0.1000	0.0270
4	35	10	0	3.25	0.00834	24.900	−0.0050	0.0291
5	30	10	0	3.00	0.02500	24.700	−0.0400	0.0290
6	40	12	0	3.00	0.02500	25.300	−0.0055	0.0271

Table A.3
Cost and emission coefficients of the thermal generators for TS-3.

Gen#	P_i^{max} (MW)	P_i^{min} (MW)	a_i ($/h)	b_i ($/MWh)	$c_i(\times 0.01)$ ($/(MW^{2}h))	d_i $/h	e_i rad/MW	α_i (ton/h)	β_i (ton/MWh)	$\gamma_i(\times 0.01)$ (ton/MW^{2}h)	$\eta_i(\times 0.01)$ (ton/h)	$\delta_i(\times 0.01)$ (1/MW)
1	150	40	70.81	4.88	0.135	56.31	0.055	4.073	−2.312	5.534	0.21	3.875
2	130	35	96.13	4.56	0.522	74.77	0.043	3.216	−2.142	6.123	0.52	4.223
3	120	35	225.95	6.25	0.335	157.34	0.045	3.775	−2.021	5.785	0.65	4.756
4	110	35	217.51	6.17	0.378	147.82	0.071	3.972	−1.581	4.432	0.37	5.789
5	110	35	237.77	7.12	0.276	135.96	0.065	4.332	−2.276	6.395	0.43	6.773
6	120	35	318.21	7.74	0.417	196.33	0.053	4.112	−1.943	5.295	0.56	3.156

Table B.1
Mean values of active load demands (MW) for TS-1 to TS-3.

Bus#	P_d	Bus#	P_d	Bus#	P_d	Bus#	P_d	Bus#	P_d	Bus#	P_d
1	0	6	0	11	0	16	3.5	21	17.5	26	3.5
2	21.7	7	22.8	12	11.2	17	9	22	0	27	0
3	2.4	8	30	13	0	18	3.2	23	3.2	28	0
4	7.6	9	0	14	6.2	19	9.5	24	8.7	29	2.4
5	94.2	10	5.8	15	8.2	20	2.2	25	0	30	10.6

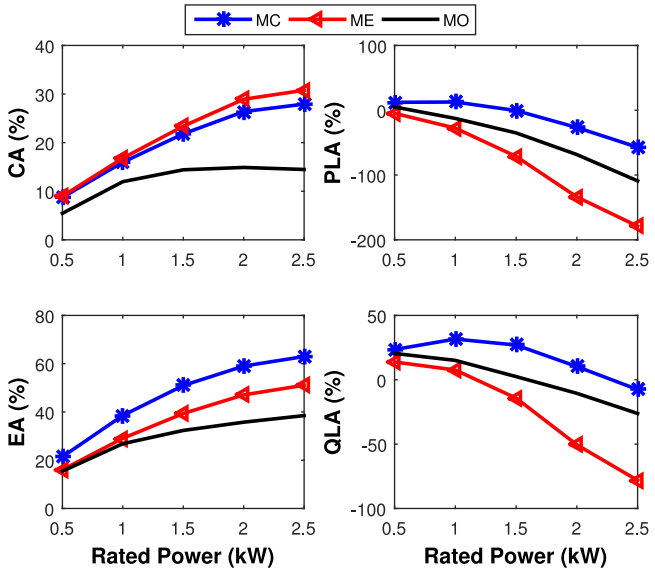

Fig. 22. Additionality in TS-2 (Scenario-6).

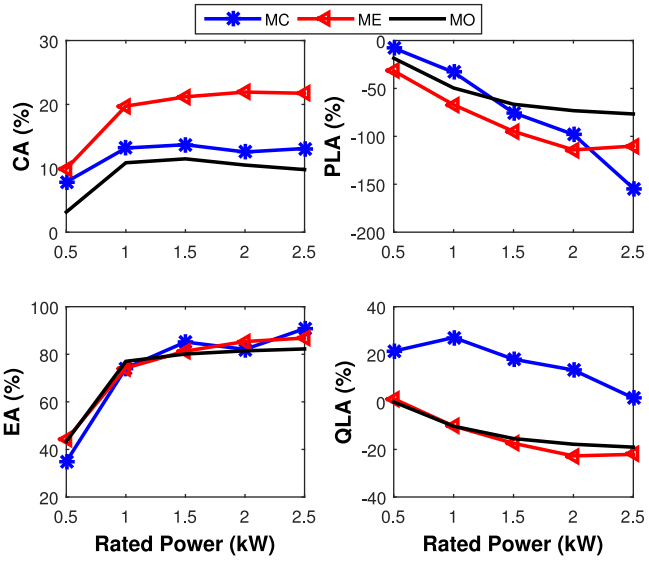

Fig. 23. Additionality in TS-3 (Scenario-6).

5.7. Summary of results

The following points are worth noting from the above discussion.

1. The variation in additionality is dependent on the location at which the wind farm is integrated.
2. A change in P_r changes the additionality of the wind farms, however, this sensitivity varies across test systems.
3. A change in v_r and hence TPI also affects the additionality of the wind farms but this effect is much less pronounced compared to change in P_r.

Table B.2
Mean values of active load demands (MW) for TS-4.

Bus#	P_d	Bus#	P_d	Bus#	P_d	Bus#	P_d	Bus#	P_d	Bus#	P_d	Bus#	P_d	Bus#	P_d
1	51	16	25	31	43	46	28	61	0	76	68	91	10	106	43
2	20	17	11	32	59	47	34	62	77	77	61	92	65	107	50
3	39	18	60	33	23	48	20	63	0	78	71	93	12	108	2
4	39	19	45	34	59	49	87	64	0	79	39	94	30	109	8
5	0	20	18	35	33	50	17	65	0	80	130	95	42	110	39
6	52	21	14	36	31	51	17	66	39	81	0	96	38	111	0
7	19	22	10	37	0	52	18	67	28	82	54	97	15	112	68
8	28	23	7	38	0	53	23	68	0	83	20	98	34	113	6
9	0	24	13	39	27	54	113	69	0	84	11	99	42	114	8
10	0	25	0	40	66	55	63	70	66	85	24	100	37	115	22
11	70	26	0	41	37	56	84	71	0	86	21	101	22	116	184
12	47	27	71	42	96	57	12	72	12	87	0	102	5	117	20
13	34	28	17	43	18	58	12	73	6	88	48	103	23	118	33
14	14	29	24	44	16	59	277	74	68	89	0	104	38	–	–
15	90	30	0	45	53	60	78	75	47	90	163	105	31	–	–

4. The additionality of the wind farms in power systems is governed by the fuel cost and emission characteristics of the thermal generators.
5. The variation in additionality do not vary much between scenarios with only wind variation and those with both wind and load variations provided the uncertainty is weighted equally between both.

6. Conclusion

In this work, the importance of additionality is emphasized as the capability of the wind farm to reduce the fuel cost and emission of the existing thermal generators. The corresponding trade-off in terms of network losses is also highlighted. This work is pioneering in visualizing the traditional operational parameters of the power systems as attributes of the wind farm. The impact of power systems on the cost, emission, real power losses and reactive power losses are investigated. Wind farms of similar capacity are incorporated in four different test power systems. It is found that the location of the wind farms in the power systems do influence the additionality of the wind farms. The additionality is also greatly influenced by the fuel cost and emission characteristics of the existing generators. Further, it is found that influence on additionality is quite sensitive to the change in turbine ratings especially the rated power of the turbine. These results are significant in the sense that the additionality terms calculated during project planning stage may be quite different when the wind farms are integrated in the power system. Therefore, at the early stage of preparation of project design document, this aspect needs to be incorporated to have a realistic measure of the additionality of the wind farms. As a future work, other operational costs and reactive power limits of the generators can be incorporated in additionality evaluation of wind farms.

Appendix A. Cost and emission coefficients

See Tables A.1–A.3.

Appendix B. Mean values of active load demand P_d

See Tables B.1 and B.2.

References

[1] United Nations Millennium Development Goals. [Online]. Available: http://www.un.org/millenniumgoals/environ.shtml.
[2] Clean Development Mechanism. [Online]. Available: https://cdm.unfccc.int/about/index.html.
[3] Thomas Ackermann, Wind Power in Power Systems, John Wiley and Sons Ltd, 2005.
[4] Christy Nguyen, Chunbo Ma, Atakelty Hailu, Morteza Chalak, Factors influencing calculation of capacity value of wind power: A case study of the Australian National Electricity Market (NEM), Renew. Energy (ISSN: 0960-1481) 90 (2016) 319–328, http://dx.doi.org/10.1016/j.renene.2016.01.007.
[5] Mark Capellaro, Prediction of site specific wind energy value factors, Renew. Energy (ISSN: 0960-1481) 87 (Part I) (2016) 430–436, http://dx.doi.org/10.1016/j.renene.2015.10.019.
[6] Intended Nationally Determined Contributions. [Online]. Available: http://www4.unfccc.int/submissions/INDC/Submission%20/submissions.aspx.
[7] CDM Methodologies. [Online]. Available: https://cdm.unfccc.int/methodologies/index.html.
[8] CDM Project Activities. [Online]. Available: https://cdm.unfccc.int/Projects/registered.html.
[9] Ghazale Haddadian, Nasrin Khalili, Mohammad Khodayar, Mohammad Shahidehpour, Optimal coordination of variable renewable resources and electric vehicles as distributed storage for energy sustainability, Sustain. Energy Grids Netw. (ISSN: 2352-4677) 6 (2016) 14–24, http://dx.doi.org/10.1016/j.segan.2015.12.001.
[10] M. Xu, A. Wilson, C.J. Dent, Calibration and sensitivity analysis of long-term generation investment models using Bayesian emulation, Sustain. Energy Grids Netw. (ISSN: 2352-4677) 5 (2016) 58–69, http://dx.doi.org/10.1016/j.segan.2015.10.007.
[11] Hossam A. Gabbar, Aboelsood Zidan, Optimal scheduling of interconnected micro energy grids with multiple fuel options, Sustain. Energy Grids Netw. (ISSN: 2352-4677) 7 (2016) 80–89, http://dx.doi.org/10.1016/j.segan.2016.06.006.
[12] Vivek Mohan, Jai Govind Singh, Weerakorn Ongsakul, M. Madhu Nimal, M.P. Reshma Suresh, Economic and network feasible online power management for renewable energy integrated smart microgrid, Sustain. Energy Grids Netw. (ISSN: 2352-4677) 7 (2016) 13–24, http://dx.doi.org/10.1016/j.segan.2016.04.003.
[13] Andrés Feijóo, Daniel Villanueva, Assessing wind speed simulation methods, Renew. Sustain. Energy Rev. 56 (2016) 473–483.
[14] Kasra Mohammadi, Omid Alavi, Ali Mostafaeipour, Navid Goudarzi, Mahdi Jalilvand, Assessing different parameters estimation methods of Weibull distribution to compute wind power density, Energy Convers. Manage. 108 (15) (2016) 322–335.
[15] Kasra Mohammadi, Omid Alavi, Jon G. McGowan, Use of Birnbaum-Saunders distribution for estimating wind speed and wind power probability distributions: A review, Energy Convers. Manage. (ISSN: 0196-8904) 143 (2017) 109–122, http://dx.doi.org/10.1016/j.enconman.2017.03.083.
[16] Rajat Kanti Samal, Manish Tripathy, Estimating wind speed probability distribution based on measured data at Burla in Odisha, India, Energy Sources, Part A (2018) http://dx.doi.org/10.1080/15567036.2018.1521888.
[17] A. Fabbri, T.G.S. Roman, J.R. Abbad, V.H.M. Quezada, Assessment of the cost associated with wind generation prediction errors in a liberalized electricity market, IEEE Trans. Power Syst. 20 (3) (2005) 1440–1446, http://dx.doi.org/10.1109/TPWRS.2005.852148.
[18] Fan Liu, Zhaohong Bie, Shiyu Liu, Tao Ding, Day-ahead optimal dispatch for wind integrated power system considering zonal reserve requirements, Appl. Energy (ISSN: 0306-2619) 188 (2017) 399–408, http://dx.doi.org/10.1016/j.apenergy.2016.11.102.
[19] Guzmán Díaz, Javier Gómez-Aleixandre, José Coto, Wind power scenario generation through state-space specifications for uncertainty analysis of wind power plants, Appl. Energy (ISSN: 0306-2619) 162 (2016) 21–30, http://dx.doi.org/10.1016/j.apenergy.2015.10.052.
[20] Zhiwen Wang, Chen Shen, Feng Liu, A conditional model of wind power forecast errors and its application in scenario generation, Appl. Energy (ISSN: 0306-2619) 212 (2018) 771–785, http://dx.doi.org/10.1016/j.apenergy.2017.12.039.

[21] Shanshan Pan, Jinbao Jian, Linfeng Yang, A hybrid MILP and IPM approach for dynamic economic dispatch with valve-point effects, Int. J. Electr. Power Energy Syst. (ISSN: 0142-0615) 97 (2018) 290–298, http://dx.doi.org/10.1016/j.ijepes.2017.11.004.
[22] J. Hetzer, D.C. Yu, K. Bhattarai, An economic dispatch model incorporating wind power, IEEE Trans. Energy Convers. 23 (2) (2008) 603–611.
[23] Shanhe Jiang, Zhicheng Ji, Yan Wang, A novel gravitational acceleration enhanced particle swarm optimization algorithm for wind–thermal economic emission dispatch problem considering wind power availability, Int. J. Electr. Power Energy Syst. 73 (2015) 1035–1050.
[24] Manjaree Pandit, Vishal Chaudhary, Hari Mohan Dubey, B.K. Panigrahi, Multi-period wind integrated optimal dispatch using series PSO-DE with time-varying Gaussian membership function based fuzzy selection, Int. J. Electr. Power Energy Syst. (ISSN: 0142-0615) 73 (2015) 259–272, http://dx.doi.org/10.1016/j.ijepes.2015.05.017.
[25] J.M. Lujano-Rojas, G.J. Osório, J.P.S. Catalão, New probabilistic method for solving economic dispatch and unit commitment problems incorporating uncertainty due to renewable energy integration, Int. J. Electr. Power Energy Syst. (ISSN: 0142-0615) 78 (2016) 61–71, http://dx.doi.org/10.1016/j.ijepes.2015.11.064.
[26] Jingliang Jin, Peng Zhou, Mingming Zhang, Xianyu Yu, Hao Din, Balancing low-carbon power dispatching strategy for wind power integrated system, Energy (ISSN: 0360-5442) 149 (2018) 914–924, http://dx.doi.org/10.1016/j.energy.2018.02.103.
[27] M. Pirnia, C.A. Cañizares, K. Bhattacharya, A. Vaccaro, A novel affine arithmetic method to solve optimal power flow problems with uncertainties, IEEE Trans. Power Syst. 29 (6) (2014) 2775–2783.
[28] Julio Usaola, Probabilistic load flow with correlated wind power injections, Electric Power Syst. Res. (ISSN: 0378-7796) 80 (5) (2010) 528–536, http://dx.doi.org/10.1016/j.epsr.2009.10.023.
[29] Jia Cao, Zheng Yan, Probabilistic optimal power flow considering dependences of wind speed among wind farms by pair-copula method, Int. J. Electr. Power Energy Syst. 84 (2017) 296–307.
[30] Ambarish Panda, M. Tripathy, Security constrained optimal power flow solution of wind-thermal generation system using modified bacteria foraging algorithm, Energy (ISSN: 0360-5442) 93 (Part 1) (2015) 816–827, http://dx.doi.org/10.1016/j.energy.2015.09.083.
[31] Chun-Lien Su, Probabilistic load-flow computation using point estimate method, IEEE Trans. Power Syst. 20 (4) (2005) 1843–1851, http://dx.doi.org/10.1109/TPWRS.2005.857921.
[32] Chun-Lien Su, Chan-Nan Lu, Two-point estimate method for quantifying transfer capability uncertainty, IEEE Trans. Power Syst. 20 (2) (2005) 573–579, http://dx.doi.org/10.1109/TPWRS.2005.846233.
[33] M. Mohammadi, A. Shayegani, H. Adaminejad, A new approach of point estimate method for probabilistic load flow, Int. J. Electr. Power Energy Syst. (ISSN: 0142-0615) 51 (2013) 54–60, http://dx.doi.org/10.1016/j.ijepes.2013.02.019.
[34] C. Delgado, J.A. Domínguez-Navarro, Point estimate method for probabilistic load flow of an unbalanced power distribution system with correlated wind and solar sources, Int. J. Electr. Power Energy Syst. (ISSN: 0142-0615) 61 (2014) 267–278, http://dx.doi.org/10.1016/j.ijepes.2014.03.055.
[35] Xue Li, Jia Cao, Dajun Du, Probabilistic optimal power flow for power systems considering wind uncertainty and load correlation, Neurocomputing (ISSN: 0925-2312) 148 (2015) 240–247, http://dx.doi.org/10.1016/j.neucom.2013.09.066.
[36] Qing Xiao, Comparing three methods for solving probabilistic optimal power flow, Electric Power Syst. Res. (ISSN: 0378-7796) 124 (2015) 92–99, http://dx.doi.org/10.1016/j.epsr.2015.03.001.
[37] Seyed Masoud Mohseni-Bonab, Abbas Rabiee, Behnam Mohammadi-Ivatloo, Saeid Jalilzadeh, Sayyad Nojavan, A two-point estimate method for uncertainty modeling in multi-objective optimal reactive power dispatch problem, Int. J. Electr. Power Energy Syst. (ISSN: 0142-0615) 75 (2016) 194–204, http://dx.doi.org/10.1016/j.ijepes.2015.08.009.
[38] S. Surender Reddy, Optimal scheduling of thermal-wind-solar power system with storage, Renew. Energy (ISSN: 0960-1481) 101 (2017) 1357–1368, http://dx.doi.org/10.1016/j.renene.2016.10.022.
[39] Can Chen, Wenchuan Wu, Boming Zhang, Hongbin Sun, Correlated probabilistic load flow using a point estimate method with Nataf transformation, Int. J. Electr. Power Energy Syst. (ISSN: 0142-0615) 65 (2015) 325–333, http://dx.doi.org/10.1016/j.ijepes.2014.10.035.
[40] S. Shargh, B. Khorshid ghazani, B. Mohammadi-ivatloo, H. Seyedi, M. Abapour, Probabilistic multi-objective optimal power flow considering correlated wind power and load uncertainties, Renewable Energy (ISSN: 0960-1481) 94 (2016) 10–21, http://dx.doi.org/10.1016/j.renene.2016.02.064.
[41] C.S. Saunders, Point estimate method addressing correlated wind power for probabilistic optimal power flow, IEEE Trans. Power Syst. 29 (3) (2014) 1045–1054, http://dx.doi.org/10.1109/TPWRS.2013.2288701.
[42] Rajat Kanti Samal, M. Tripathy, Cost savings and emission reduction capability of wind-integrated power systems, Int. J. Electr. Power Energy Syst. (ISSN: 0142-0615) 104 (2019) 549–561, http://dx.doi.org/10.1016/j.ijepes.2018.07.039.
[43] Giovanni Gualtieri, Sauro Secci, Methods to extrapolate wind resource to the turbine hub height based on power law: A 1-h wind speed vs. Weibull distribution extrapolation comparison, Renewable Energy (ISSN: 0960-1481) 43 (2012) 183–200, http://dx.doi.org/10.1016/j.renene.2011.12.022.
[44] Vinay Thapar, Gayatri Agnihotri, Vinod Krishna Sethi, Critical analysis of methods for mathematical modelling of wind turbines, Renew. Energy (ISSN: 0960-1481) 36 (11) (2011) 3166–3177, http://dx.doi.org/10.1016/j.renene.2011.03.016.
[45] S.H. Jangamshetti, V. Guruprasada Rau, Normalized power curves as a tool for identification of optimum wind turbine generator parameters, IEEE Trans. Energy Convers. 16 (3) (2001) 283–288.
[46] MATPOWER, A MATLAB Power System Simulation Package, Online. Available: http://www.pserc.cornell.edu/matpower/.
[47] Data for 118 Bus Test System. [Online]. Available: motor.ece.iit.edu/data/SCUC_118test.xls [accessed 2018].